

## Supporting Information

### Heteroatom Substituted Zeolite FAU with Ultralow Al Contents for Liquid-Phase Oxidation Catalysis

Daniel T. Bregante,<sup>‡</sup> Jun Zhi Tan,<sup>‡</sup> Andre Sutrisno,<sup>†</sup> and David W. Flaherty<sup>‡,\*</sup>

<sup>‡</sup>*Department of Chemical and Biomolecular Engineering*

<sup>†</sup>*NMR/EPR Laboratory at the School of Chemical Sciences*

*University of Illinois at Urbana-Champaign, Urbana, IL 61801, USA*

\*Corresponding Author

Phone: +1 217-244-2816

Email: [dwflhrty@illinois.edu](mailto:dwflhrty@illinois.edu)

## S1.0 Characterization of Ti-BEA, Ti-SiO<sub>2</sub>, and TS-1

### S1.1 X-ray Diffraction of Ti-BEA and TS-1

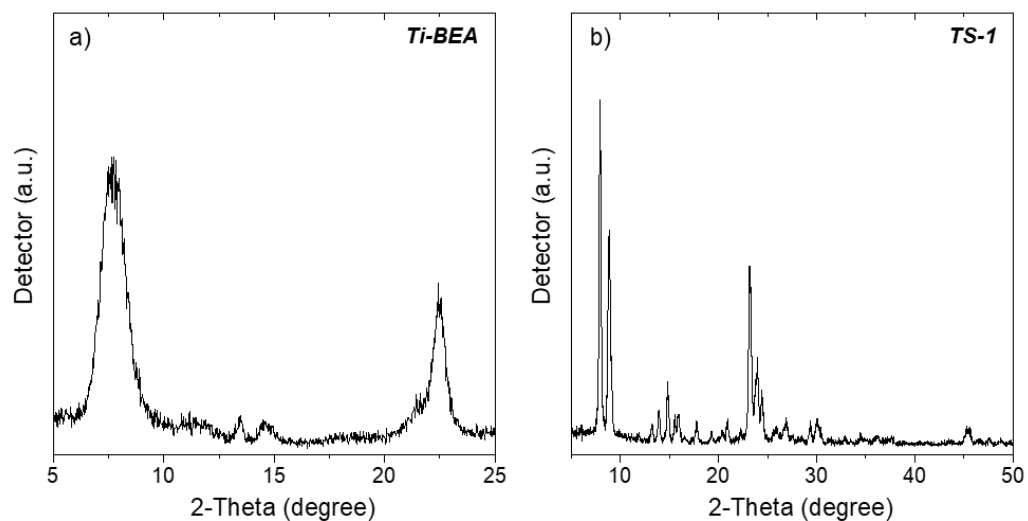


**Figure S1.** X-ray diffractograms of (a) Ti-BEA and (b) TS-1.

Figure S1 shows X-ray diffractograms for Ti-BEA and TS-1, which indicate that these materials contain diffraction features characteristic of the BEA and MFI zeolite frameworks, respectively.

## S1.2 Diffuse Reflectance UV-vis of Ti-BEA, Ti-SiO<sub>2</sub>, and TS-1

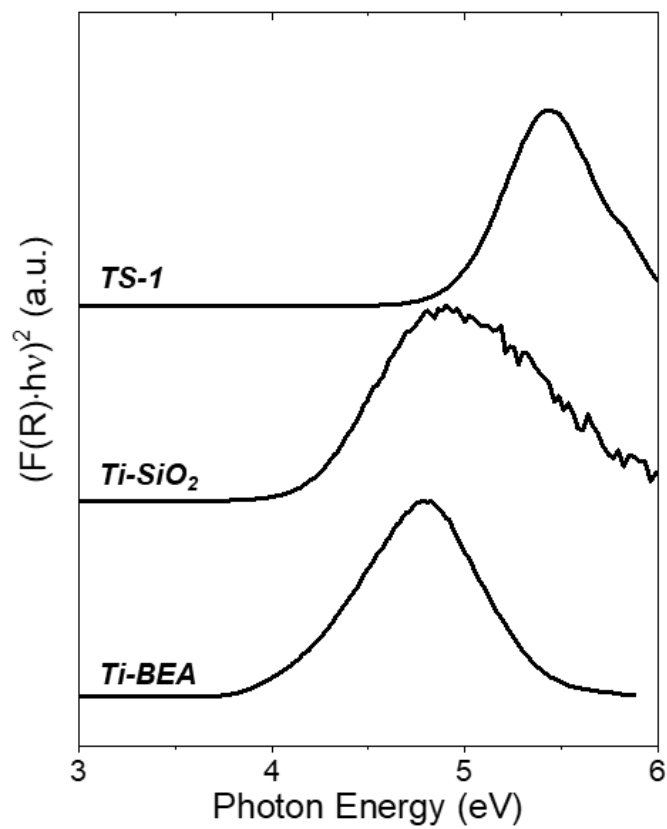


**Figure S2.** Tauc plots for Ti-BEA, Ti-SiO<sub>2</sub>, and TS-1. Note that  $F(R)$  corresponds to the Kubelka-Munk pseudo-absorbance. All spectra were normalized to the most-intense feature and are vertically offset for clarity.

## S2.0 M-FAU Characterization

### S2.1 X-Ray Diffraction to Show Changes in Lattice Spacing

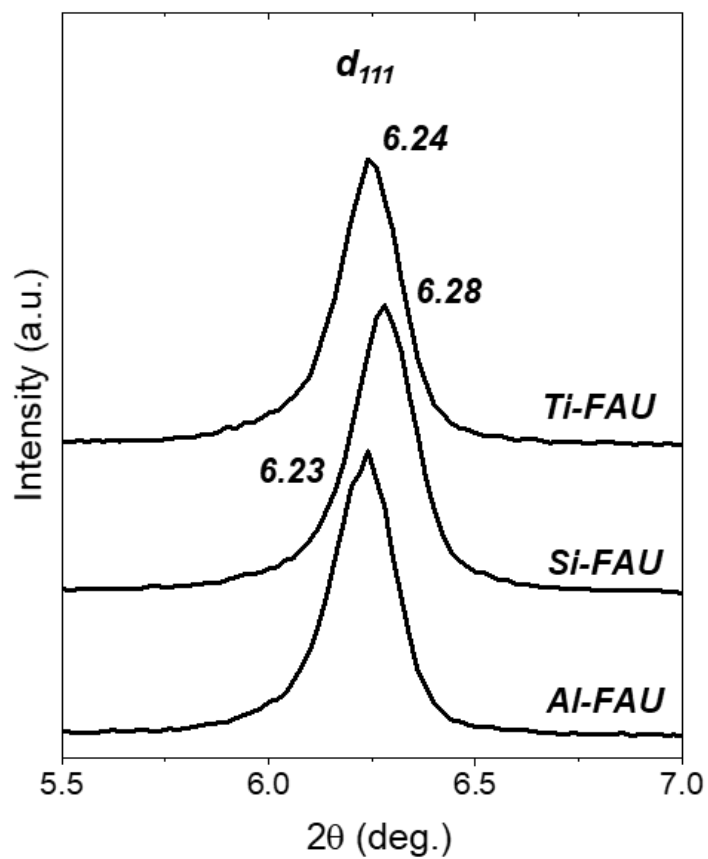


**Figure S3.** X-ray diffractograms for Al-, Si-, and Ti-FAU. Diffractograms are vertically offset for clarity.

## S2.2 Nitrogen Volumetric Adsorption to Show Isotherm Type

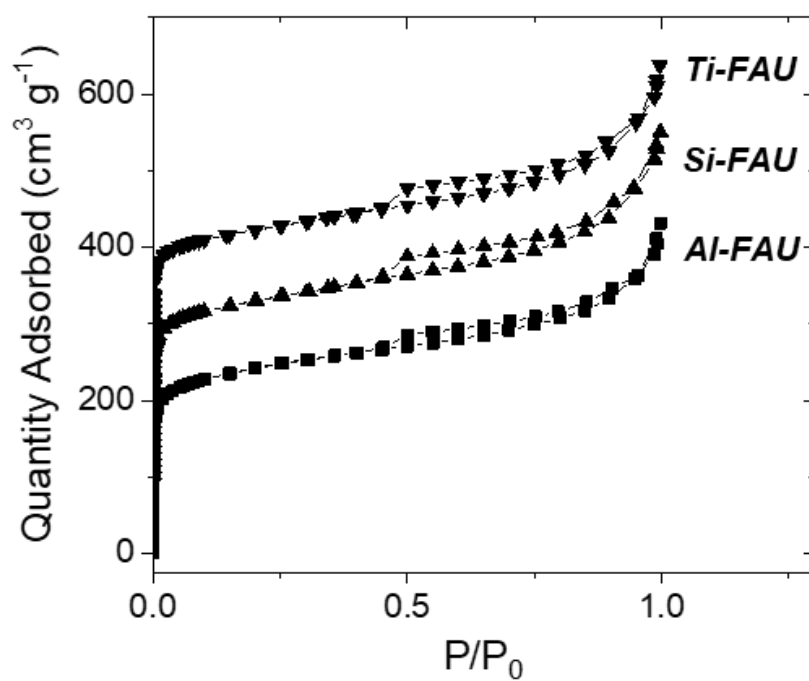


**Figure S4.** Nitrogen adsorption isotherms (77 K) for Al-, Si-, and Ti-FAU. Adsorption isotherms are offset for clarity.

### S2.3 $^{29}\text{Si}$ MAS-NMR Spectra to Visualize $\text{Q}^4$ Features

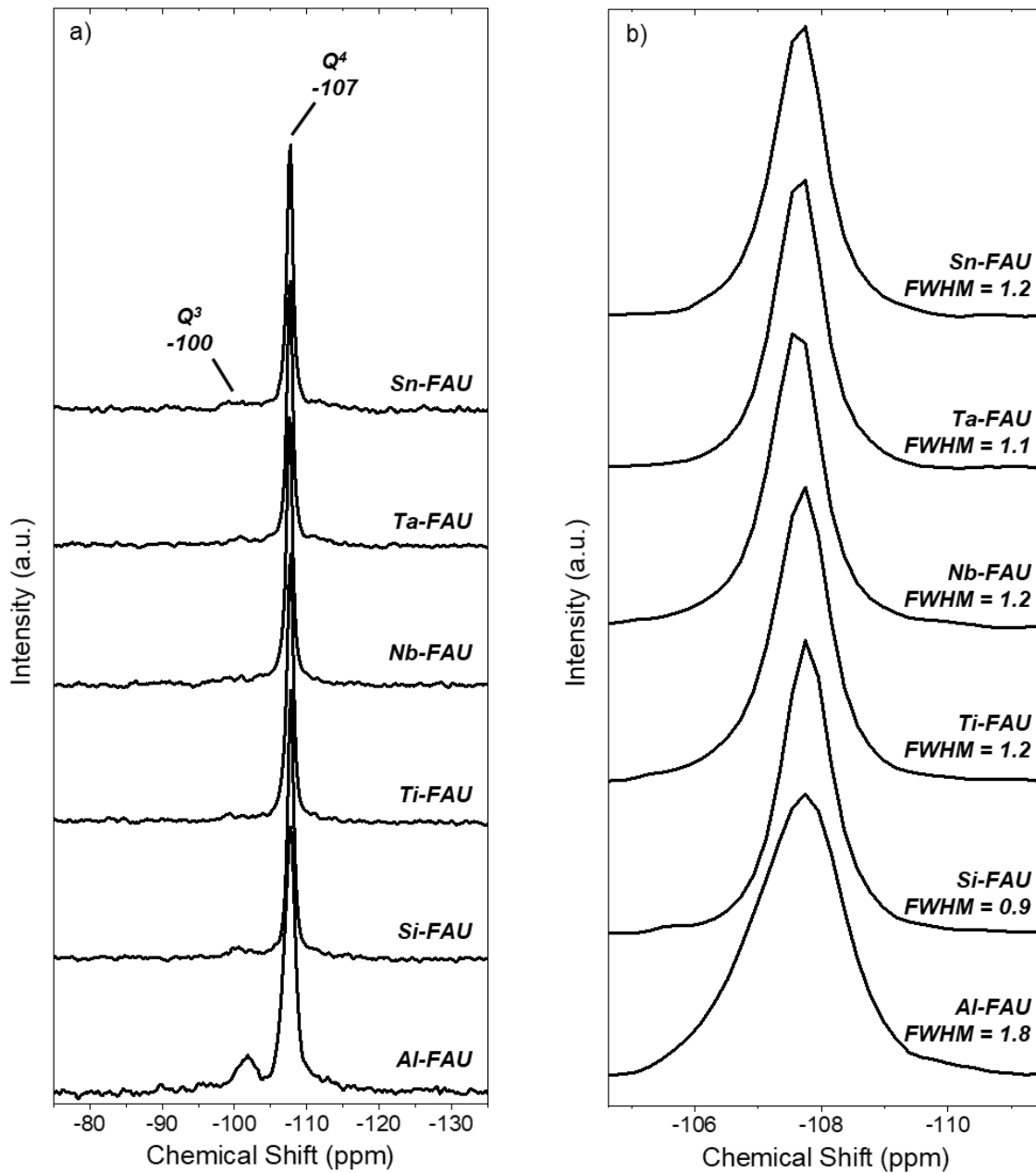


**Figure S5.** (a)  $^{29}\text{Si}$  direct polarization MAS-NMR spectra of Al-, Si-, Ti-, Nb-, Ta-, and Sn-FAU. Panel (b) shows changes in the full width-half max (FWHM) of the  $\text{Q}^4$  features within each M-FAU. All spectra are normalized to the  $\text{Q}^4$  feature and are offset for clarity.

### S3.0 Peak Fitting Procedures

#### S3.1 $^{29}\text{Si}$ MAS-NMR of Si-FAU Example Peak Fitting

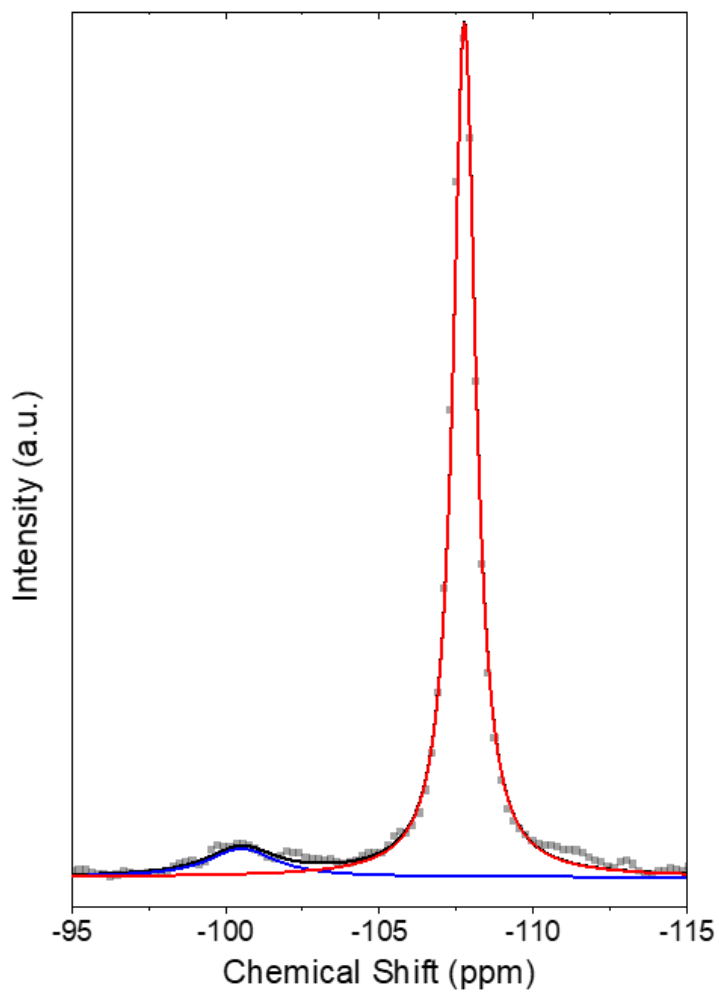


**Figure S6.** Example peak fitting procedure for  $^{29}\text{Si}$  MAS-NMR spectra (gray ■) of Si-FAU. The red curve represents NMR features attributed to  $\text{Q}^4$  sites, while the blue curve represents those belonging to  $\text{Q}^3$  sites; the black curve is the cumulative fit. In all cases, Lorentzian curves were used for the fitting procedure. Values of  $\phi_{\text{NMR}}$  were estimated by dividing the area under the blue curve to that of the black curve.

### S3.2 Infrared Spectroscopy of Dehydrated Si-FAU Example Peak Fitting

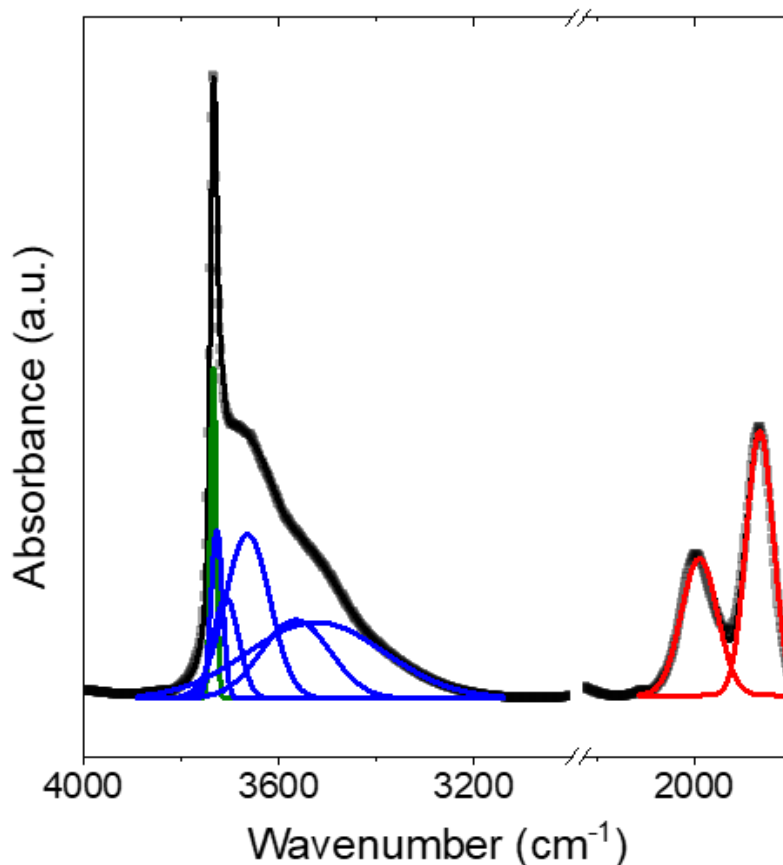


**Figure S7.** Infrared spectra (gray ■) of dehydrated Si-FAU (573 K, He). Gaussian curves were used to fit the data in all cases. The green curve represents  $\nu(\text{O-H})$  of isolated SiOH, the blue curves are  $\nu(\text{O-H})$  resulting from hydrogen-bonded SiOH (e.g.,  $(\text{SiOH})_4$ ), and red curves represent  $\nu(\text{Si-O-Si})$  overtone stretches. The black curves represent cumulative fits.

Six gaussian curves were chosen to fit the infrared spectra of M-FAU in order to capture the proper curvature and yield a  $R^2$  value  $>0.995$ . Fitting procedures using three-to-five gaussian curves yielded nearly identical values of  $\phi_{\text{IR}}$ .



## S4.0 Epoxidation of 2,4-dimethylstyrene

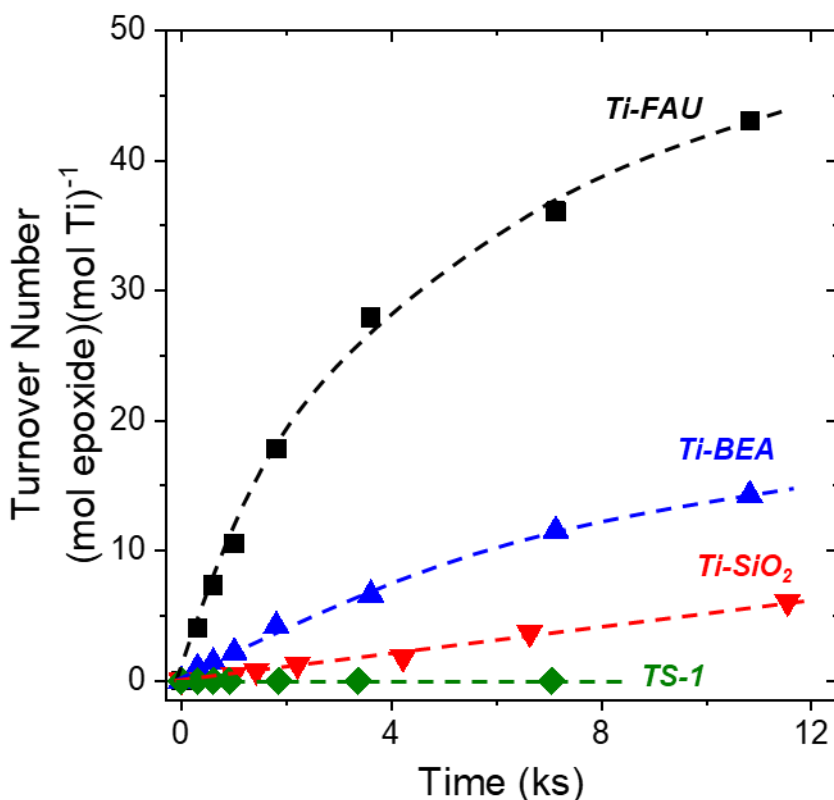


**Figure S8.** Turnover numbers as a function of time for the epoxidation of 2,4-dimethylstyrene (0.1 M 2,4-dimethylstyrene, 0.1 M H<sub>2</sub>O<sub>2</sub>, in CH<sub>3</sub>CN, 313 K) over Ti-FAU (black ■), Ti-BEA (blue ▲), Ti-SiO<sub>2</sub> (red ▼), and TS-1 (green ◆). Dashed curves are intended to guide the eye.

Figure S8 shows the turnover numbers for 2,4-dimethylstyrene epoxidation over Ti-FAU, Ti-BEA, Ti-SiO<sub>2</sub>, and TS-1. Turnover numbers (and rates) for 2,4-dimethylstyrene epoxidation are greatest within Ti-FAU and decrease in the order Ti-BEA, Ti-SiO<sub>2</sub>, and TS-1. Notably, rates of 2,4-dimethylstyrene epoxidation are immeasurable on TS-1 because TS-1 possesses pores that are 0.55 nm in diameter, which is smaller than the kinetic diameter of 2,4-dimethylstyrene (e.g., *m*-xylene has a kinetic diameter of 0.68 nm),<sup>1</sup> which precludes the diffusion and reaction of 2,4-dimethylstyrene within the MFI framework. The increased turnover numbers for 2,4-dimethylstyrene oxide formation within Ti-FAU relates to the increased entropic freedom of the transition state for epoxidation within Ti-FAU compared to Ti-BEA, with the increased enthalpic stabilization relative to Ti-SiO<sub>2</sub>.

## **References:**

1. M. Jahandar Lashaki, M. Fayaz, S. Niknaddaf and Z. Hashisho, *J. Hazard. Mater.*, 2012, **241-242**, 154-163.